COBEM 2023 27TH INTERNATIONAL CONGRESS OF MECHANICAL ENGENEERING

ABCM Brazilian Society of Mechanical Sciences and Engineering
27th ABCM International Congress of Mechanical Engineering
December 04-08, 2023, Florianópolis-SC, Brazil

COB-2023-2028
AERODYNAMIC ANALYSIS APPLIED TO A HYPERSONIC VEHICLE TYPE WAVERIDER THROUGH CFD

Rolando Guzmán-Bohórquez
Paulo Celso Greco Júnior
Hernán Dario Cerón-Muñoz
Department of Aeronautical Engineering, São Carlos School of Engineering, University of São Paulo - Avenida João Dagnone, 1100, Jd. Santa Angelina - CEP 13563-120 - São Carlos - SP.
rolandoguzmanbohorquez@usp.br
pgreco@sc.usp.br
hernan@sc.usp.br

Abstract. *Hypersonic aerodynamics has had a huge interest since its beginnings stemming from all the particular phenomena encountered at very high-speed flight conditions. In the last decades, this practical interest has been increasing due to the possible applications, not only in transport but also in the military field. Nowadays, applied hypersonic aerodynamics captures the attention for the design and development of vehicles that could offer better performance with such conditions at the extreme end of the whole flight spectrum. The waverider is a lifting body, which has an attached shock wave all along its leading edge, producing more lift at lower angles of attack than generic hypersonic vehicles. In this sense, waveriders possess a higher lift-to-drag ratio (L/D) than other hypersonic vehicles. The maximum L/D for a flight vehicle is a measure of its aerodynamic efficiency. That is the reason why the waverider is a promising candidate as a base design for feasible hypersonic vehicles. This paper aims to carry out an aerodynamic analysis of a wedge-derived waverider model, which is based on a previously obtained model through meta-heuristic methods of optimization that attempted to maximize both the aerodynamic efficiency and the payload, characterized by the L/D ratio and the internal volume of the vehicle, respectively. The methodology adopted to do this type of analysis was by solving the governing flow equations for the flow field numerically, through the use of a computational fluid dynamics (CFD) commercial software. Inviscid and viscous CFD simulations were performed to investigate the influence of the inflow at free-stream Mach numbers of $M_\infty = 5$, $M_\infty = 6$, and $M_\infty = 7$ and the angle of attack on the vehicle ($AoA = 0°$). The objective was to examine the aerodynamic performance in terms of quantitative characteristics such as lift and drag and identify qualitative features such as the boundary layer and shock layer thickness and their respective behaviors, besides the interaction between the boundary layer and the outer inviscid flow, commonly known as viscous interaction. The obtained results are intended to help the generation of a preliminary aerodynamic database and in addition, to validate the obtained waverider models. Therefore, the study of these kinds of optimal preliminary designs of a generalized waverider is of utmost importance as a conceptual basis for the designers of the next hypersonic vehicles, considering that it provides a foreseeable behavior of the vehicle and the flow phenomena present around it.*

Keywords: *Aerodynamics, Hypersonics, Hypersonic Vehicle, Waverider.*

1. INTRODUCTION

Nowadays, it seems that the major aircraft manufacturers have defined three features to implement in their product design as a standard: to have higher efficiency, a reasonable price, and moreover to be environmentally safe or "eco-friendly". Nonetheless, there are other kinds of requirements that are worth taking into consideration besides the sustainable, economic, and ecological aspects. The minimization of traveling time is one of them. For this reason, hypersonic vehicles have been acquiring even more interest lately, since their conception. As a matter of fact, traveling from Tokyo to Los Angeles in just 110 minutes is possible using hypersonic transport (Taguchi *et al.*, 2008). Characteristics such as high speed, among several others, could definitely have a radical impact on the conceptual design and development of the new tailor-made vehicles and the feasible applications that these could have for both, commercial and military purposes, as stated by Sziroczak and Smith (2016).

In this respect, aerodynamic-based design is a fundamental part of any aircraft development process, since it is directly related to the flight performance and quality of the whole vehicle and also it has an impact on flight safety, economy, and efficiency (Zhao *et al.*, 2020). Usually, the aerodynamic efficiency is measured in terms of the maximum lift-to-drag ratio (L/D_{max}) for a flight vehicle. But, by misfortune, for supersonic and hypersonic flight vehicles, the higher the freestream Mach number, the lower L/D_{max}. This is just natural behavior at these high-speed conditions, caused by the sudden increase of strength in the shock waves and the consequent wave drag increment as the Mach number increases,

explains Anderson (2011). In a few words, for vehicles flying at hypersonic flight Mach numbers, the L/D value is low, which could be inconvenient for future hypersonic vehicles intended to fly in the atmosphere.

However, there exists a type of base form for hypersonic vehicles which produces higher values in terms of L/D than other generic vehicles: waveriders. "A waverider is a supersonic or hypersonic vehicle that has an attached shock wave all along its leading edge", defines Anderson (2011, p. 910). The aerodynamic advantage of having the shock wave attached to the lower surface is that this high pressure does not leak around the leading edge to the upper surface, i.e. more lift is generated because that flow acting over the lower surface is contained and so the high pressure is held back. On account of that, it is as if the vehicle is riding on top of its shock wave, therefore the coined term: “waverider”.

Nonweiler (1959) was the first to introduce the concept of waverider through the generation of “caret-shaped waveriders” from the two-dimensional flow field behind a planar oblique shock wave created by a wedge. Moreover, Nonweiler had a particular interest in such waveriders, commonly designated by the symbol "$\wedge$", as lifting atmospheric entry bodies. Then, there was an extension of the concept developed by Nonweiler, using a conical-generating flow by Jones (1963). In addition, other extensions applying axisymmetric generating flows were addressed by Jones *et al.* (1968). Rasmussen (1980) and his colleagues at the University of Oklahoma (Kim *et al.*, 1983)(Broadaway, 1983), used the hypersonic small-disturbance theory for the design of waveriders from both flow fields over right-circular cones and elliptic cones. What is more, Rasmussen was able to make use of the classic calculus of variations seeking to optimize the waverider shapes utilizing the inviscid properties of the flow. Afterwards, Anderson and his students at the University of Maryland (Capriotti, 1987)(Bowcutt *et al.*, 1987) generated new families of waveriders, in which the skin-friction drag was taken into account in their optimization routines to calculate waveriders with maximum L/D. This family of waveriders is called viscous-optimization hypersonic waveriders, and subsequent CFD calculations and wind-tunnel tests have proven their viability, thus significantly enhancing modern interest in the waverider concept, as affirm Anderson (2011).

Even so, given the highly interconnected nature of waverider design, it is really challenging to perform an optimization including different fields of interest with the traditional methodologies. For a real waverider design process enclosing topics like the wide-body and payload, lifting and control surfaces, and intake and exhaust stages of the propulsion system among others, the usage of Multidisciplinary Design Optimization (MDO) schemes is required (Silva *et al.*, 2021). Various techniques have been used in different elements in the optimization of a hypersonic vehicle with diverse focuses. e.g. Peng *et al.* (2019) achieved the optimal shape that satisfies payload size constraints, improving the aerodynamic performance of the hypersonic vehicle through an analytic method combined with a clamped cubic spline curve. Viviani *et al.* (2020) aimed to optimize the shape of hypersonic re-entry vehicles using a multi-objective evolutionary algorithm. While, Chen *et al.* (2020) made an optimization applied to an axisymmetric hypersonic vehicle, coupling the global optimization algorithms $NSGA-II$ with a CFD fluid analysis in order to find configurations with a better performance.

Despite other multiple authors have conducted studies concerning aerodynamic optimization, it was not seen methodology that has involved within the multi-objective optimization, the comparison between two or more different optimization methods, just the research of Silva *et al.* (2021), whose main objective was through meta-heuristic computational optimization methods obtain optimal preliminary designs of a generalized wedge-derived waverider configuration relating coefficients based on geometric constraints and aerodynamic efficiency. Now that such optimal wedge-derived waverider geometries were obtained for the aerodynamic efficiency and payload fuselage, it becomes mandatory that such models are subjected to a process of validation, taking into account the constraints under which they were optimized and the objective values for which they were planned to perform. Here is where it lies the main objective of the present research. At this starting point, it is taken one of the representatives obtained geometries by Silva *et al.* (2021), whose design was pretended to obtain mid values for both the aerodynamic efficiency and the payload volume. Based on such a model, it is generated another geometry with similar topological parameters. This new wedge-derived waverider model is intended to be assessed aerodynamically, with the usage of CFD. Inviscid and Viscous simulations are performed with the objective of analyzing and determining aerodynamic parameters at a different M_∞, besides identifying behaviors and phenomena present in both the shock layer and boundary layer and in the surroundings of the vehicle. This article presents the proposed and implemented methodology for the simulations of the flow field around such waverider, the obtained results with its respective analysis, and the conclusions drawn from it.

2. METHODOLOGY

2.1 Waverider Geometry

The waverider design is an inverse process, meaning the best vehicle shape is created for a specific flow field. The requirements of the flow field are met by this geometry. The following inputs are needed for the design process (based on an inviscid flow field): Generation of a shock surface, definition of the vehicle leading edge on the generating shock surface, free-stream Mach number $M_\infty = M_{design}$, and shock angle of the generating shock surface. Then, the stream surface emanating from the specified leading edge determines the lower side of a waverider. The shock surface is consequently attached to this leading edge. Since shockwave downstream pressure is increased, this stream surface produces the shape lift and the corresponding wave drag. Therefore, one of the primary goals of an optimization process is to achieve the

maximum aerodynamic performance L/D for a specific Mach number (Hirschel and Weiland, 2009).

One of the optimal waverider models obtained by Silva *et al.* (2021) through the use of metaheuristic (MH) methods was chosen to apply the methodology in order to carry the study out: the model which was obtained for mid values of L/D and V. Based on this waverider, an identical geometry is generated taking into account the topological parameters of the original one, as is presented in Fig. 1. Taking as reference the research developed by Ferguson *et al.* (2015), Li *et al.* (2017), and Moran *et al.* (2023) the sharp leading edge of the model is modified by means of the blunt method for waverider configuration. The bluntness round measure is defined according to the 0.1% of L, where L is the characteristic length of the waverider.

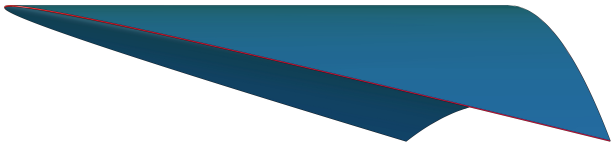

Figure 1: Waverider geometry.

2.2 Flow Parameters and Conditions

A half-ellipsoid domain is adopted surrounding the waverider geometry and using the longitudinal axis of the vehicle as the symmetry reference. An unstructured mesh of tetrahedral elements is generated with a second body of refinement near the vehicle surface with the intention of capturing the entire shock layer for various M_∞. The computational domain and its meshing are shown in Fig. 2. In order to investigate the effect of grid-scale, the grid convergence is analyzed, which is presented in the Tab. 1 including the grid size of different scales in terms of element quantity. The simulation of convergence analysis is performed in an inviscid condition at a $M_\infty = 5$. The L/D parameter was chosen, and in consequence, the C_L and C_D, as parameters of interest. Because of the percent difference between the considered grid cases in terms of L/D, the moderate grid is selected for the simulations since it lasts $1/3$ of the time required by the refined grid with just a difference of 0.00974% in the obtained values for L/D, which infers a good accuracy in the obtained results and computational resource performance.

Table 1: Grid convergence analysis.

Cases	**Grid Size**	$\boldsymbol{C_L}$	$\boldsymbol{C_D}$	$\boldsymbol{L/D}$
Coarse	$1,116,015$	0.057871	0.007570	7.644782
Moderate	$2,870,250$	0.057872	0.007572	7.642894
Refined	$5,663,273$	0.057874	0.007573	7.642149

(a) Domain.

(b) Meshed Domain.

Figure 2: Computational domain.

Not only inviscid but also viscous numerical simulations were performed aiming to assess the aerodynamic performance of the studied waverider. The correspondent cases are listed in Tab. 2 and are classified in agreement with the M_∞ and the turbulence model.

Table 2: Cases classification according to M_∞ and model.

Case	M_∞	**Model**
1	5	$Inviscid$
2	6	$Inviscid$
3	7	$Inviscid$
4	5	$Viscous : (k\omega SST)$
5	6	$Viscous : (k\omega SST)$
6	7	$Viscous : (k\omega SST)$

The freestream conditions were stipulated according to an ($H = 30km$) of the International Standard Atmosphere (ISA), as can be appreciated in the Tab. 3. The other conditions could be obtained by means of the correlation of these conditions at a given altitude. The boundary conditions imposed on the computational domain are based on the work of Chen *et al.* (2020): while the pressure outlet boundary condition is chosen for the outlet, the pressure far-field boundary condition is specified for the inflow, and the waverider surface boundary condition is set as an adiabatic wall with no slip.

Table 3: Free stream conditions for the numerical simulations.

Case	M_∞	$\alpha[°]$	$H[km]$	$T_\infty[K]$	$P_\infty[Pa]$
All	$5, 6, 7$	0	30	231.83	1151.4

To complete the simulation numerically, the simulation platform chosen is the commercial CFD software ANSYS Fluent. The density-based solver is used to solve the three-dimensional implicit coupled Reynolds Averaged Navier-Stokes ($RANS$) and Euler equations and obtain the desired outcomes. Because it offers a precise resolution of contact and shock discontinuities and is less prone to Carbuncle phenomena, the second-order spatially Advection Upstream Splitting Method ($AUSM$) to the flux vector is used, according to Chen *et al.* (2019). The $k\omega - SST$ turbulent model is chosen to obtain the viscous results, and the least-squares cell-based approach is chosen to compute the gradients. The Courant-Friedrichs-Levy (CFL) number is set at 0.5 with proper under-relaxation factors to ensure stability. The air is assumed to be a thermally and calorically perfect gas because air is compressible in hypersonic flow. The viscosity coefficient μ is determined using Sutherland law, and the specific heat ratio γ is taken to be a constant value of 1.4.

The convergence parameters for either inviscid or viscous simulations were chosen for the residuals to achieve the $1e^{-4}$ order and the C_L and C_D reach a steady state. Moreover, 10,000 iterations were defined for the numerical simulations whether or not the previous conditions were met, based on the research developed by Moran *et al.* (2023).

3. RESULTS

After the numerical simulations cases were performed in the computational resources and the solution of the governing flow equations (Euler and $RANS$) were reached, it proceeded to analyze the obtained outcomes and to visualize the fluid flow behavior over the vehicle.

3.1 Qualitative Results

Figure 3, Fig. 4, and Fig. 5 provide the pressure contours at the base plane of the vehicle, along with the inviscid and viscous findings, for a more thorough analysis of the flow field features. It is evident that the waverider design is able to restrict the high pressure of the lower surface when both inviscid and viscous computations are used, and the waverider properties are preserved, satisfying the "better aerodynamic performance" requirement, given that the flow under the pressure surface i.e. the lower one, is preserved.

Nevertheless, it is observed too that near the zone of the leading edge occurs a fluid leakage of low pressure that is in consonance with the shock cone and therefore with the shock layer. It could be appreciated that the higher the M_∞ case, the thinner the shock layer is. Also, an almost planar-attached shock wave is contained in the lower surface, which is a distinctive feature of the wedge-derived waveriders. It is important to stand out that including the viscous effects, a slightly bigger shock cone is generated for the same geometry and the pressure effects are even more distinguishable in comparison with the inviscid cases. For that reason, it is fundamental to keep in mind that for each exposed case, a pressure convention range is established. In addition, the low-pressure zones for all the cases are mainly concentrated

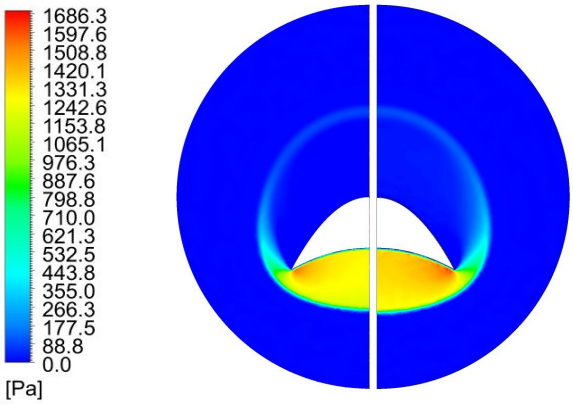

(a) Inviscid (b) Viscous

Figure 3: Comparison of pressure contours at the base plane between cases 1 and 4 ($M_\infty = 5$).

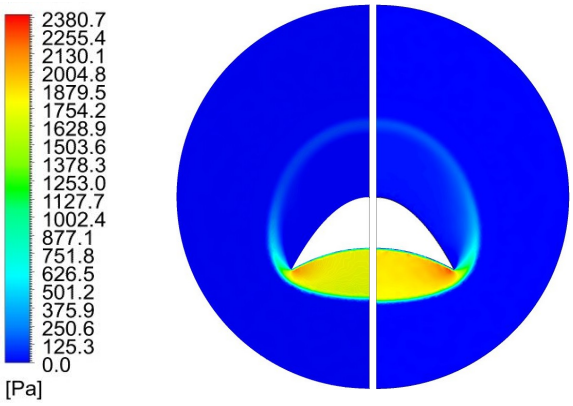

(a) Inviscid (b) Viscous

Figure 4: Comparison of pressure contours at the base plane between cases 2 and 5 ($M_\infty = 6$).

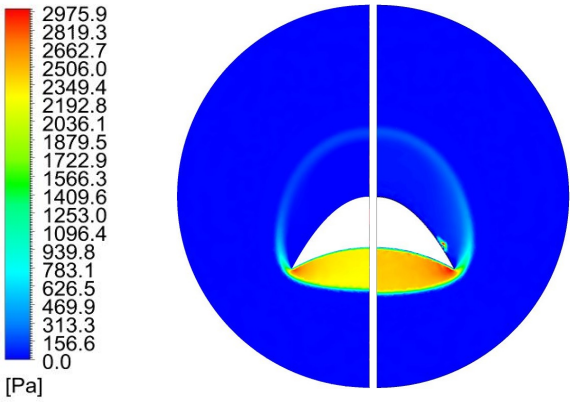

(a) Inviscid (b) Viscous

Figure 5: Comparison of pressure contours at the base plane between cases 3 and 6 ($M_\infty = 7$).

in the median region of the lower surface, while the high-pressure region for all the cases is located on both sides of the lower surface, attached under the leading edge. To complete the analysis, it is identified a particular little zone over the upper surface in the viscous case for a $M_\infty = 7$ (Fig. 5b), which presents a high-pressure characteristic.

The obtained Mach number results in the symmetry plane of the domain exhibit the relation of the waverider vehicle velocity with respect to the sound velocity at given conditions. Figure 6, Fig. 7, and Fig. 8 show a comparison of the outcomes in terms of Mach contours at the study defined M_∞'s, whose main characteristic is the visualization of the shock layer and the shock waves generated up and down the vehicle geometry. It is worth highlighting that the Mach number has a defined range for every exposed comparison case. One of the main features that could be observed is the generation of the boundary layer over the model surface for the viscous cases and the absence of it in the inviscid ones. That is because in the inviscid ones just lie the presence of the pressure forces whilst in the viscous ones, not only the pressure forces are present, but also the forces owing to the viscous forces.

A fascinating aspect of these figures is that the reduction of the shock layer size as the M_∞ gets increased can be perceptible. i.e. the higher the Mach, the smaller the size of the shock layer, which aligns with the physics of this flight regime. Not only that, the boundary layer becomes more noticeable and wider as the M_∞ gets increased. Such a physical phenomenon is confirmed by the numerical simulation outcomes, probably by means of the entropy layer and the viscous interaction, which are common characteristics of the physical behavior of the hypersonic flow. Besides the fact that the inviscid flow outer the boundary layer but inner the shock layer is identified too.

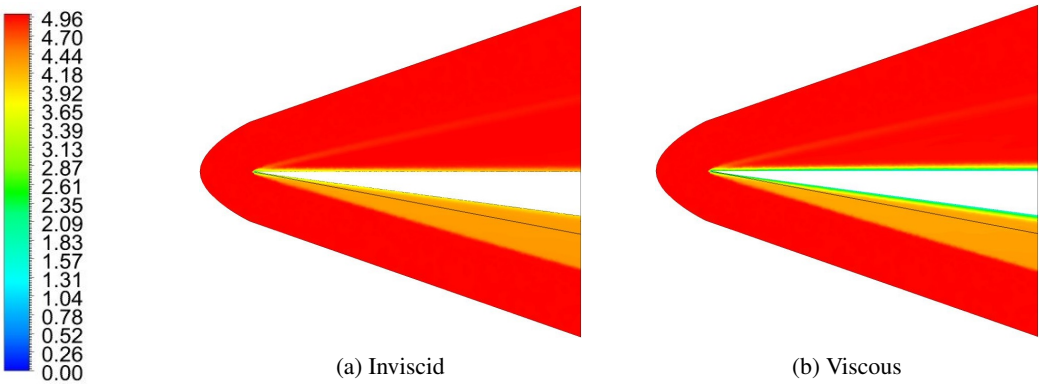

(a) Inviscid (b) Viscous

Figure 6: Comparison of mach contours at the symmetry plane between cases 1 and 4 ($M_\infty = 5$).

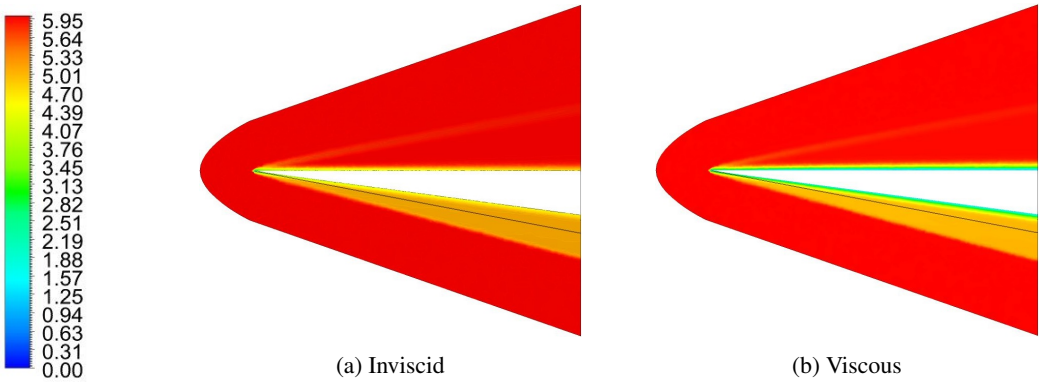

(a) Inviscid (b) Viscous

Figure 7: Comparison of mach contours at the symmetry plane between cases 2 and 5 ($M_\infty = 6$).

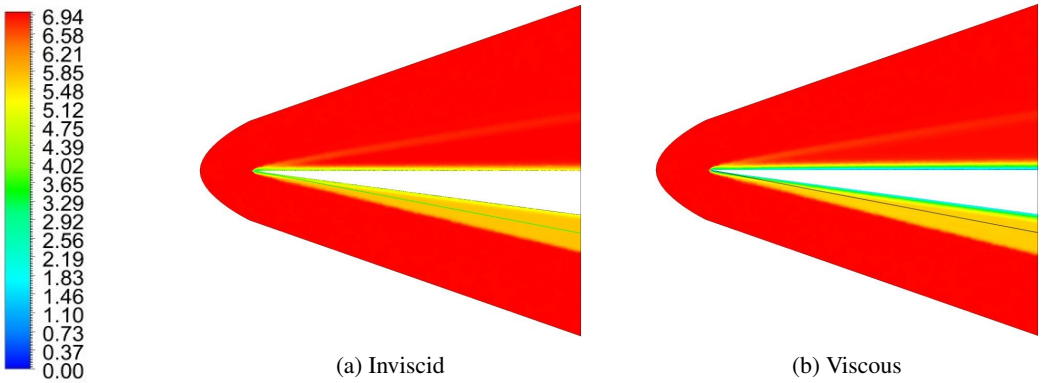

(a) Inviscid (b) Viscous

Figure 8: Comparison of mach contours at the symmetry plane between cases 3 and 6 ($M_\infty = 7$).

3.2 Quantitative Results

Regarding the quantitative aerodynamic aspects, the obtained outcome values: C_L, C_D, and L/D are listed in Tab. 4 for every studied case. However, their behavior is even more perceptible in a graphic manner. For account of that, Fig. 9 is presented, in which could be looked that the viscous obtained values for C_L and C_D lie above the inviscid ones, but still keep a similar tendency to decrease when the M_∞ rises, which it is the expected behavior.

Now then, making an assessment of the L/D of the vehicle at various M_∞, the behavior changes. The current behavior in terms of L/D is almost constant and its variation is tiny with a slight tendency to decrease as the M_∞ rises.

Table 4: Aerodynamic parameters obtained from numerical simulations for each case.

Case	M_∞	C_L	C_D	L/D
1	5	0.05793	0.00757	7.64933
2	6	0.05320	0.00704	7.55217
3	7	0.04962	0.00662	7.48588
4	5	0.05888	0.01230	4.78522
5	6	0.05460	0.01150	4.74709
6	7	0.05121	0.01084	4.72288

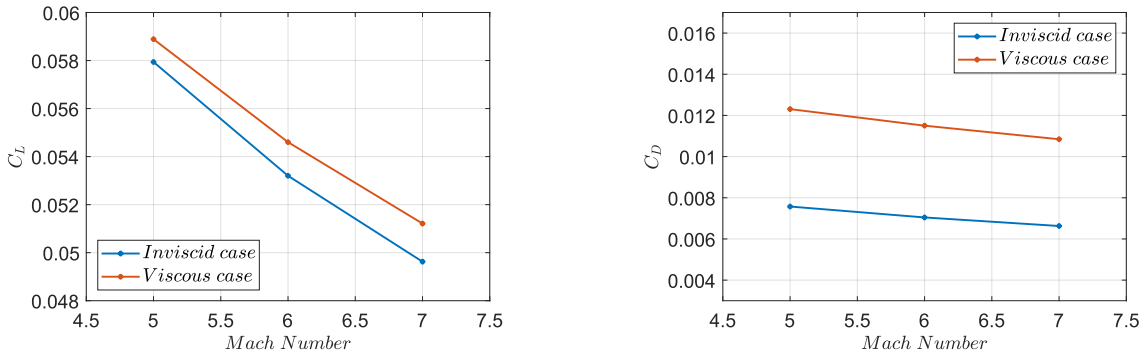

(a) Lift coefficient (b) Drag coefficient

Figure 9: Comparison of aerodynamic parameters at different M_∞.

This behavior could be appreciated in Fig: 10b. This trend can be compared with other relations encountered in the literature. In this way, Anderson (2011) states that "for supersonic and hypersonic vehicles, L/D markedly decreases as M_∞ increases". In fact, based on real flight-vehicle experience, Küchemann (2012) provides the general empirical correlation for $(L/D)_{max}$ in Eq. (1). Whilst, the more accurate expression in Eq. (2) describes the L/D variation of the viscous optimized waveriders (Anderson, 2011).

$$(L/D)_{\max} = \frac{4\,(M_\infty + 3)}{M_\infty} \tag{1}$$

$$(L/D)_{\max} = \frac{6\,(M_\infty + 2)}{M_\infty} \tag{2}$$

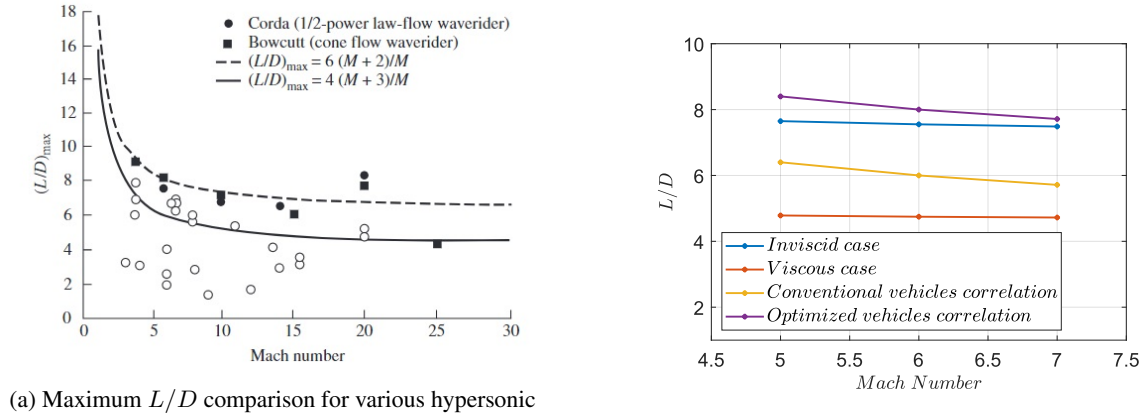

(a) Maximum L/D comparison for various hypersonic configurations, (Anderson, 2011)

(b) L/D obtained and reference correlation values

Figure 10: Lift-to-drag ratio comparison at different M_∞.

The solid Kuchemann curve in Fig. 10a illustrates a particular kind of "L/D barrier" that is challenging to overcome for conventional vehicles. Figure 10a displays open circles that correspond to data for different conventional vehicles,

which reflect different wind tunnel and flying tests. The solid symbols correspond to different optimized hypersonic waveriders: solid circles represent results for a different family of viscous optimized waveriders based on the shock wave and downstream stream surfaces generated by a one-half power law ogive-shaped body, while solid squares represent results for waveriders based on conical generating flows. It is evident that the viscous optimized waveriders provide L/D_{max} values that are above the Kuchemann curve, breaking the L/D barrier. The dashed curve in Fig. 10a represents this variation. The findings in that figure demonstrate the significance of the viscous optimized waveriders. These findings have been verified by multiple wind tunnel experiments. They are the cause of the resurgence of interest in the waverider configuration for use as a hypersonic vehicle, especially for extended atmospheric cruising, established Anderson (2011). Because of that, it is that the obtained L/D for the studied waverider is compared against these two correlation trends, for the conventional hypersonic vehicles and the optimized ones, as can be appreciated in Fig. 10b.

3.3 Discussion

In order to make a conscientious analysis of the obtained aerodynamic data, Tab. 5 presents the percentage variation for the C_L, C_D, and L/D parameters while the M_∞ increases, this in relation to the immediate previous Mach obtained value.

Table 5: Progressive percentage difference for obtained aerodynamic parameters while M_∞ increases.

Δ Case	$C_{LInv}[\%]$	$C_{DInv}[\%]$	$L/D_{Inv}[\%]$	**Δ Case**	$C_{LVis}[\%]$	$C_{DVis}[\%]$	$L/D_{Vis}[\%]$
$\Delta_{1\to2}$	8.905	7.522	1.286	$\Delta_{4\to5}$	7.854	6.995	0.803
$\Delta_{2\to3}$	7.206	6.265	0.885	$\Delta_{5\to6}$	6.617	6.073	0.512

In addition, aiming to complement the simulation cases comparison with the classical and optimized correlations, Tab. 6 is presented. In it, it can be seen clearly the percent difference between the respective cases and the closer correlation applied to them.

Table 6: Percentage difference between obtained values of L/D with respect to the closer empirical correlation.

Case	**OVC** $L/D_{Max}[\%]$	**Case**	**CVC** $L/D_{Max}[\%]$
1	9.813	**4**	33.745
2	5.929	**5**	26.393
3	3.051	**6**	20.991

4. CONCLUSIONS

For the assessed waverider, these conclusions were drawn:

The pressure contours generated at the base plane of the vehicle have shown interesting differences between the inviscid and viscous cases. First of all, the shock cone is bigger in the inviscid case. On the other hand, despite the highest-pressure concentration being located under and near the waverider leading edge, this concentration is more notorious for the inviscid cases. Also, the shock wave is almost flattened in the limit cone region under the vehicle compression surface.

The boundary layer observed in the Mach contours for the viscous cases is more evident as the M_∞ is increased. In the same way, the higher the Mach, the thinner the shock layer. Regarding that, the viscous interaction between the thicker boundary layer and the inviscid flow inner the shock layer is appreciated for each case.

The C_L and C_D tendency at a different M_∞ is of decrement in a range between the 6% and 9% for both the inviscid and viscous simulations. Moreover, the viscous values for the mentioned parameters lie above the inviscid ones in a pretty similar tendency.

The variation of the L/D for the inviscid and viscous cases is really tiny with approximately 1%. It is worth highlighting that despite there exists a correspondence between the vehicle L/D and the empirical correlations, at the evaluated Mach numbers the trend is to keep constant whilst the correlations tendency is to decrease. Also, the inviscid L/D values are closer to the optimized vehicles correlation, and because of that above the L/D viscous values.

5. ACKNOWLEDGEMENTS

This study was financed in part by the Coordenação de Aperfeiçoamento de Pessoal de Nível Superior - Brasil (CAPES) - Finance Code 001. In this respect, the first author would like to express his gratitude to CAPES, within the scope of the call PROCAD/DEFESA 2019 - Project no., 88887.387752/2019-00. Also, the authors all thank Ph.D.

Candidate J.J. Vaca-Rios - Department of Aeronautics - EESC-USP, M.Sc. H.G. Parra and Ph.D. W. Gómez - Mechatronics Department - UMNG for providing the computational resources for the numerical simulations.

6. REFERENCES

Anderson, J., 2011. *EBOOK: Fundamentals of Aerodynamics (SI Units)*. McGraw hill.

Bowcutt, K.G., Anderson, J.D. and Capriotti, D., 1987. "Numerical optimization of conical flow waveriders including detailed viscous effects". *Aerodynamics of Hypersonic Lifting Vehicles*.

Broadaway, R.T., 1983. *Aerodynamics of a Simple Cone-Derived Waverider*. Ph.D. thesis, University of Oklahoma.

Capriotti, D., 1987. "Viscous optimized hypersonic waveriders". In *25th AIAA Aerospace Sciences Meeting*. p. 272.

Chen, J., Fan, X., Xiong, B., Meng, Z. and Wang, Y., 2020. "Parameterization and optimization for the axisymmetric forebody of hypersonic vehicle". *Acta Astronautica*, Vol. 167, pp. 239–244.

Chen, L.L., Guo, Z., Deng, X., Hou, Z. and Wang, W., 2019. "Waverider Configuration Design With Variable Shock Angle". *IEEE access : practical innovations, open solutions*, Vol. PP, pp. 1–1. doi:10.1109/ACCESS.2019.2907806.

Ferguson, F., Dasque, N., Dhanasar, M. and Blankson, I., 2015. *The Design, Analysis and Performance Evaluation of Waverider Configurations for Hypersonic Vehicle Applications*. doi:10.2514/6.2015-1008.

Hirschel, E.H. and Weiland, C., 2009. *Selected Aerothermodynamic Design Problems of Hypersonic Flight Vehicles*, Vol. 229. Springer Science & Business Media.

Jones, JG., 1963. "A method for designing lifting configurations for high supersonic speeds using the flow fields of non-lifting cones". *RAE Report No. Aero 2674*.

Jones, JG., Moore, KC., Pike, J. and Roe, PL., 1968. "A method for designing lifting configurations for high supersonic speeds, using axisymmetric flow fields". *Ingenieur-Archiv*, Vol. 37, pp. 56–72.

Kim, BS., Rasmussen, ML. and Jischke, M.C., 1983. "Optimization of waverider configurations generated from axisymmetricconical flows". *Journal of Spacecraft and Rockets*, Vol. 20, No. 5, pp. 461–469.

Küchemann, D., 2012. "The Aerodynamic Design of Aircraft". In *The Aerodynamic Design of Aircraft*, American Institute of Aeronautics and Astronautics, Inc., AIAA Education Series, pp. i–xviii. ISBN 978-1-60086-922-8. doi: 10.2514/5.9781600869228.0000.0000.

Li, S.b., Wang, Z., Huang, W., Xu, S. and Yan, L., 2017. "Aerodynamic performance investigation on waverider with variable blunt radius in hypersonic flows". *Acta Astronautica*, Vol. 137. doi:10.1016/j.actaastro.2017.05.001.

Moran, J., McQuellin, L., Pollock, L., Neely, A., Munk, D. and Zander, F., 2023. *Wind-Tunnel Based Free-Flight Testing of a Viscous Optimised Hypersonic Waverider*. doi:10.2514/6.2023-1385.

Nonweiler, TRF., 1959. "Aerodynamic problems of manned space vehicles". *The Aeronautical Journal*, Vol. 63, No. 585, pp. 521–528.

Peng, W., Feng, Z. and Yang, T., 2019. "Rapid aerodynamic shape optimization with payload size constraints for hypersonic vehicle". *IEEE access : practical innovations, open solutions*, Vol. 7, pp. 84429–84447.

Rasmussen, M.L., 1980. "Waverider configurations derived from inclined circular and elliptic cones". *Journal of Spacecraft and Rockets*, Vol. 17, No. 6, pp. 537–545.

Silva, B., Paulino, A.C., Rego, I., de Oliveira, E.J. and Passaro, A., 2021. "Optimal preliminary design of hypersonic waverider using multiple metaheuristics". In *Proceedings of the 72th International Astronautical Congress - IAC 2021*. Dubai, UAE.

Sziroczak, D. and Smith, H., 2016. "A review of design issues specific to hypersonic flight vehicles". *Progress in Aerospace Sciences*, Vol. 84, pp. 1–28.

Taguchi, H., Murakami, A., Sato, T. and Tsuchiya, T., 2008. "Conceptual study on hypersonic airplanes using pre-cooled turbojet". In *15th AIAA International Space Planes and Hypersonic Systems and Technologies Conference*. p. 2503.

Viviani, A., Aprovitola, A., Iuspa, L. and Pezzella, G., 2020. "Aeroshape design of reusable re-entry vehicles by multidisciplinary optimization and computational fluid dynamics". *Aerospace Science and Technology*, Vol. 105, p. 106029.

Zhao, Z.t., Huang, W., Yan, L. and Yang, Y.g., 2020. "An overview of research on wide-speed range waverider configuration". *Progress in Aerospace Sciences*, Vol. 113, p. 100606.

7. RESPONSIBILITY NOTICE

The authors are solely responsible for the printed material included in this paper.